Spectral Probing of Surface Luminescence of Cubic $Lu_2O_3:Eu^{3+}$ Nanocrystals Synthesized by Hydrothermal Approach

Yanping Li,[†,‡] Jiahua Zhang,*[,†] Xia Zhang,[†] Yongshi Luo,[†] Shaozhe Lu,[†] Zhendong Hao,[†] and Xiaojun Wang[†,§]

Key Laboratory of Excited State Processes, Changchun Institute of Optics, Fine Mechanics and Physics, Chinese Academy of Sciences, 16 Eastern South Lake Road, Changchun 130033, China, Graduate School of Chinese Academy of Sciences, Beijing 100039, China, and Department of Physics, Georgia Southern University, Statesboro, Georgia 30460

Received: July 16, 2009; Revised Manuscript Received: August 31, 2009

Cubic $Lu_2O_3:Eu^{3+}$ nanorods, nanosheets, and nanoparticles are synthesized by a hydrothermal approach by adjusting the pH values of the precursor solutions. The unique luminescence properties of the nanocrystals are presented by the appearances of a long tail at the long-wavelength side of the charge transfer band (CTB), a novel $^7F_0-^5D_0$ broad line, and the enhanced 624 nm emission line. The observed phenomena are more obvious with decreasing sample size in the order of nanorods > nanosheets > nanoparticles. Based on the experimental results of the thermal diffusion processes of Eu^{3+} from the surface to the inside of Lu_2O_3 particles, we conclude that the unique luminescence properties of the nanocrystals originate from the surface Eu^{3+}. By the spectral decomposition, we obtain the excitation spectra of the interior Eu^{3+} and the surface Eu^{3+} of nanocrystals. In comparison with the bulk sample, the CTB of the interior Eu^{3+} presents an obvious blue shift due to the size confinement effects, while that of the surface Eu^{3+} shows a prominent red shift due to the distorted surface environments. The shorter lifetimes of the surface Eu^{3+} compared to that of the interior Eu^{3+} further indicate the distorted local environments on the surface of the nanocrystals. The shifts and the broadening of the CTB in Eu^{3+}-doped nanocrystals can be well understood by the interior Eu^{3+} and the surface Eu^{3+}.

I. Introduction

Rare earth ions activated nanosized phosphors have received extensive attention in the past few decades because of their unique properties and potential applications in the fields of luminescence devices, optical transmission, medical diagnostics, biological fluorescence labels, etc.[1−5] This interest has been stimulated by the fact that significant changes in the structural, electronic, or optical properties have been observed with decreasing particle size.[5−18] Due to an increase of surface/volume ratio, the surface luminescence of nanosized phosphors is expected to be notable. However, little evidence is demonstrated for distinguishing the surface luminescence from overall luminescence of rare earth ions activated nanosized phosphors.

Rare earth oxides are a kind of advanced host that have been widely used as high-performance phosphors, catalysts, up-conversion materials, and other functional materials.[19−21] Among them, lutetium oxide attracts increasing attention because of its high density (9.4 g/cm^3), high atomic number of Lu ($Z = 71$), and high physical and chemical stability. Moreover, it has a band gap large enough to accommodate the energy levels of many luminescent activators. These unique features make it a convenient host lattice for some activators to form scintillators or X-ray phosphors, especially for medical scintillators.[14,21] Recently, it has been reported that this host lattice activated with Eu^{3+} ion is expected to be a promising X-ray phosphor, which may serve as an efficient X-ray detector in digital planar X-ray medical imaging since the phosphor red emission fits perfectly into the highest quantum efficiency of typical CCD arrays.[21−25] To further reduce the scattering of light within the phosphor layer and, as a result, to reduce the images blurring, more attention has been drawn to the nanosized $Lu_2O_3:Eu^{3+}$. Nanosized phosphors scatter the emitted light to a much lower degree than their micrometer-sized analogues because their dimensions are smaller than the wavelengths of the radiation created upon the impact of X-rays.[25] Therefore, it is very important to synthesize nanosized $Lu_2O_3:Eu^{3+}$ in both fundamental research and practical applications.

In recent years, nanosized $Lu_2O_3:Eu^{3+}$ with different morphologies has been synthesized by various methods, and its unique luminescence properties, such as the generation of a novel $^5D_0-^7F_2$ emission line, a red shift of the charge transfer band (CTB), and the changed fluorescence lifetimes, have been reported extensively.[12−14,20,21,24−26] However, the origin of the aforementioned phenomena still lacks a clear understanding, and most explanations simply attribute them to the surface states without enough evidence. Particularly, the mechanism of the CTB shifts of Eu^{3+} in nanosized rare earth oxides is still disputed. Igarashi et al.[9] and Zhang et al.[15] reported that the CTB in nanocrystalline $Y_2O_3:Eu^{3+}$ presents a blue shift as the particle size decreased, which is attributed to the crystallinity and size confinement effects, respectively. However, other groups[6,10,14,26−28] reported the red shift of the CTB in $(Y, Lu)_2O_3:Eu^{3+}$ nanocrystals, which is attributed to the incompact lattice, surface states, and changed local structures.

In this paper, we synthesize cubic $Lu_2O_3:Eu^{3+}$ nanorods, nanosheets, and nanoparticles by a hydrothermal approach by

* To whom correspondence should be addressed. E-mail: zhangjh@ciomp.ac.cn.
† Fine Mechanics and Physics, Chinese Academy of Sciences.
‡ Graduate School of Chinese Academy of Sciences.
§ Georgia Southern University.

10.1021/jp906738m CCC: $40.75
Published on Web 09/18/2009

adjusting the pH values of the precursor solutions. By the experiment of the thermal diffusion processes of Eu^{3+} from the surface to the inside of Lu_2O_3 particles, we confirm that the unique luminescence properties of Lu_2O_3:Eu^{3+} nanocrystals presented in this paper originate from the surface Eu^{3+}. Specially, we obtain the excitation spectra of the interior Eu^{3+} and the surface Eu^{3+} of nanocrystals by spectral decomposition. The CTB of the interior Eu^{3+} presents an obvious blue shift, while that of the surface Eu^{3+} shows a prominent red shift as compared to that of the bulk sample. The origin of the shifts and the broadening of the CTB in Eu^{3+}-doped nanocrystals are clarified.

II. Experimental Section

A. Sample Preparation. The typical synthesis of Lu_2O_3:Eu^{3+} nanocrystals via the hydrothermal approach can be described as follows: the appropriate amounts of Lu_2O_3 (4 N) and Eu_2O_3 (4 N) were dissolved in dilute nitric acid (G. R.), respectively, to get the 0.4 M $Lu(NO_3)_3$ and 0.02 M $Eu(NO_3)_3$ solutions. Then 0.5 mL of $Eu(NO_3)_3$ solution was added into 1.225 mL of $Lu(NO_3)_3$ solution. Under a thorough stirring, the pH value of this solution was adjusted to a certain value (pH = 8, 11, 12) by adding dropwise dilute ammonia solution (A. R.). After continuous stirring for 1 h, the milky colloidal solution was transferred into a closed Teflon-lined autoclave and subsequently heated to 200 °C for 3 h. As the autoclave cooled to room temperature, the precipitates were washed with deionized water several times and dried at 65 °C for 14 h in a vacuum oven. The final Lu_2O_3:2% Eu^{3+} nanocrystals were obtained by annealing the precipitates at 500 °C for 1 h in air.

For comparison, the bulk Lu_2O_3:2% Eu^{3+} sample was prepared by solid-state reaction method at 1500 °C for 5 h in air, using starting materials of Lu_2O_3 and Eu_2O_3.

B. Measurements and Characterization. Field emission scanning electron microscopy (FE-SEM) images of all samples were taken on S-4800 (Hitachi Company) electron microscopes. The crystalline structures were characterized by X-ray diffraction (XRD) (Rigaku D/max-rA power diffractometer using Cu Kα (λ = 1.541 78 Å) radiation). The excitation and emission spectra were measured with a Hitachi F-4500 spectrophotometer. For comparison, the spectra were measured at a fixed band-pass of 0.2 nm with the same instrument parameters (2.5 nm for the excitation slit, 2.5 nm for the emission slit, and 700 V for the PMT voltage). High-resolution spectra were performed with a rhodamine 6G dye pumped by the Nd:YAG laser as excitation source. The spectra were recorded by a Spex-1403 spectrometer, a photomultiplier, and a boxcar integrator and processed by a computer. In lifetime measurements, the fourth (266 nm) harmonic of an Nd:YAG laser (spectra-physics, GCR 130) was used as an excitation source, and the signals were detected with a Tektronix digital oscilloscope model (TDS 3052).

III. Results and Discussion

A. Morphology and Crystal Structure. In the hydrothermal approach synthetic process, Lu_2O_3:Eu^{3+} nanocrystals with various shapes are obtained by adjusting the pH values of the precursor solutions, as the FE-SEM images illustrate in Figure 1. When the pH is adjusted to 8, the morphology of Lu_2O_3:Eu^{3+} nanocrystals is composed of nanorods cluster, as shown in Figure 1A. These nanorods clusters are stacked with several thin nanorods orderly during the process of hydrothermal treatment and annealing, and the thin nanorods are about 1 μm in length and 30 nm in diameter (see Figure 1A inset). When the pH increases to 11, the morphology of nanocrystals can change into square nanosheets completely, as shown in Figure 1B. Their side lengths are nearly 200 nm, and the thickness is 20 nm or below. Let us note that there are many "abnormally" growing square nanosheets in the products, and some sides of these "abnormal" nanosheets seemly to lose partly (see Figure 1B inset). The growth process of the nanosheets, called "side wrapping", is based on the morphologies of several intermediate nanosheets with one or two sides losing partly.[13] If the pH is continuously increased to 12, the uniform nanoparticles with the diameters of about 6 nm are obtained, as shown in Figure 1C. In Figure 1, it is illustrated clearly that the average sizes of the samples decrease in the order of nanorods > nanosheets > nanoparticles.

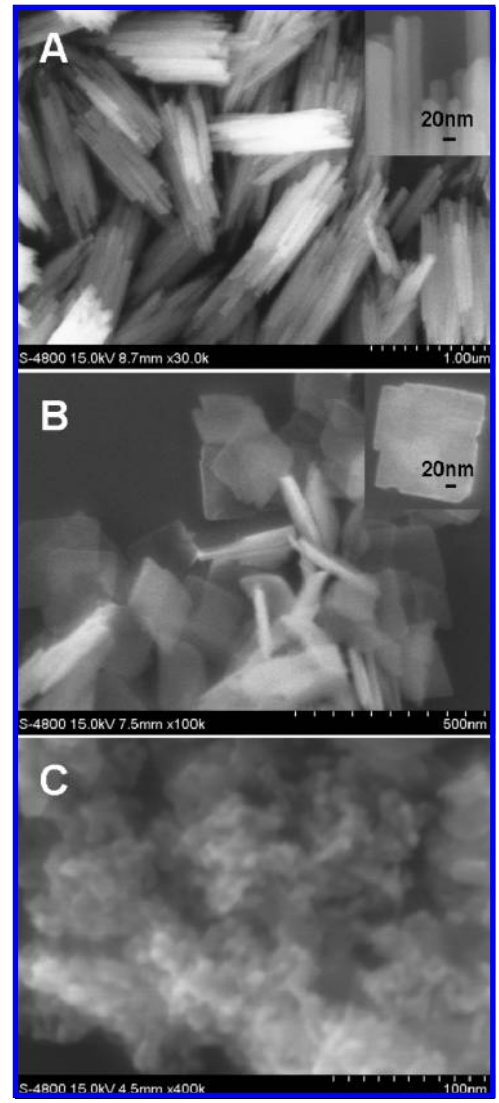

Figure 1. (A, B, and C) FE-SEM images of Lu_2O_3:Eu^{3+} nanocrystals, corresponding to pH = 8, 11, and 12, respectively.

Figure 2 displays the XRD patterns of Lu_2O_3:Eu^{3+} nanocrystals and bulk sample which are indexed to the pure cubic phase (JCPDS No. 862475). One can find that the XRD peaks become broader and broader in the order of bulk < nanorods < nanosheets < nanoparticles. This clearly reflects the descending size of the samples from the bulk to the nanoparticles, consistent with the results of the FE-SEM images as illustrated in Figure 1.

B. Photoluminescence Properties. Figure 3a shows the excitation spectra monitoring the $^5D_0-^7F_2$ emission peaking at 609 nm in Lu_2O_3:Eu^{3+} nanocrystals and bulk sample. The broad

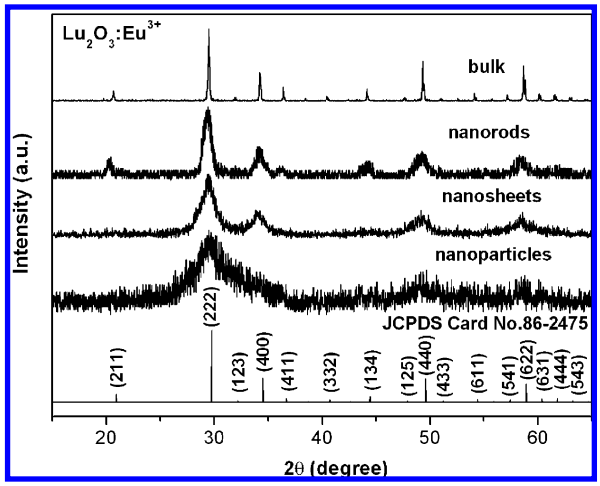

Figure 2. XRD patterns of all samples.

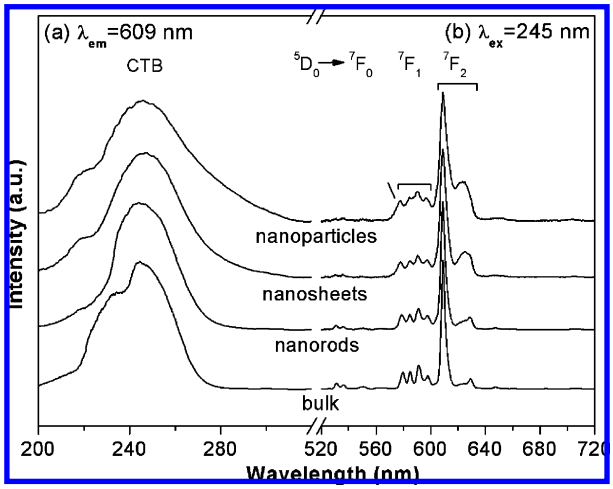

Figure 3. Excitation spectra (a) and emission spectra (b) of $Lu_2O_3:Eu^{3+}$ nanocrystals and bulk sample.

excitation band in the region of 220−310 nm is assigned to the $O^{2-}-Eu^{3+}$ charge transfer band (CTB).[21,26] It is clearly observed that the CTBs of the samples are continuously broadened and followed by a longer and longer tail at the long-wavelength side, as the samples change from the bulk sample to the nanorods, the nanosheets, and finally the nanoparticles. Thus the tail in the nanoparticles is most noticeable. The long excitation tail of the CTB has also been observed in $LuBO_3:Eu^{3+}$ nanocrystals in our previous work.[29] The excitation tail is not considered to be related to the shapes of the nanocrystals, but reasonably related to the size of the samples. Figure 3a exhibits that the CTB tail is enhanced as the sample size is reduced.

Figure 3b shows the emission spectra under 245 nm excitation in $Lu_2O_3:Eu^{3+}$ nanocrystals and bulk sample. All the spectra feature the typical emission of Eu^{3+} ions in the cubic Lu_2O_3.[26] Similar to the CTB tail, the emission line at around 624 nm originating from the $^5D_0-^7F_2$ transition of Eu^{3+} also enhances with respect to the 609 nm emission line as the sample size is reduced. The enhanced 624 nm emission line was also reported by other groups.[14,26] The spectral variation in the nanosamples indicates the generation of a novel environment in the nanosized $Lu_2O_3:Eu^{3+}$ samples. To understand if the 624 nm emission line and the CTB long tail originate from the same type of novel environment, series emission spectra are measured as shown in Figure 4.

Parts a, b, and c of Figure 4 show the emission spectra of nanorods, nanosheets, and nanoparticles, respectively, under

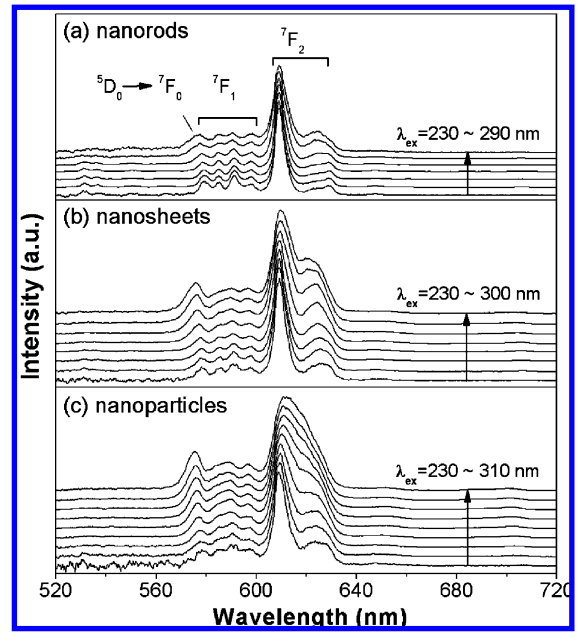

Figure 4. Emission spectra of $Lu_2O_3:Eu^{3+}$ nanorods (a), nanosheets (b), and nanoparticles (c) excited by various wavelengths within its CTB. The space of two adjacent excitation wavelengths is 10 nm.

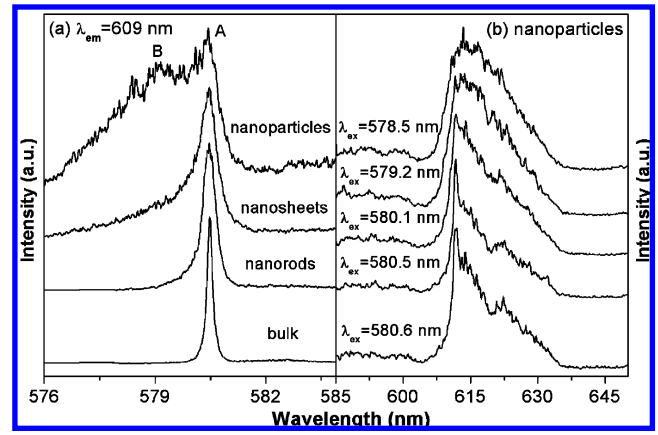

Figure 5. Excitation spectra monitoring $^5D_0-^7F_2$ emission line (λ_{em} = 609 nm) while $^7F_0-^5D_0$ is scanned in $Lu_2O_3:Eu^{3+}$ nanocrystals and bulk sample (a), and $^5D_0-^7F_2$ emission spectra of the nanoparticles as excited by different wavelengths within the $^7F_0-^5D_0$ inhomogeneous profile (b).

excitation at various wavelengths within the CTB including its long tail. It is found in all samples that the 624 nm emission line enhances notably, leading to broadening of the $^5D_0-^7F_2$ emission when the excitation wavelengths are tuned from a short-wavelength side of the CTBs to the tails. This definitely indicates that the 624 nm emission line and the CTB tail originate from the same novel type of environment. In Figure 4, it is also observed that the $^5D_0-^7F_0$ emission line grows up and shifts to the high-energy side with increasing excitation wavelengths within the CTBs. It implies the novel environment affects the $^5D_0-^7F_0$ emission property.

Considering $^5D_0$ as a nondegenerate state, we have measured the excitation spectra by collectively monitoring $^5D_0-^7F_2$ emissions and scanning the $^7F_0-^5D_0$ transition of Eu^{3+}, as shown in Figure 5a. A sharp and symmetric line at 580.5 nm (labeled A) is observed in the bulk sample. In the nanocrystals, the intrinsic line A becomes broadened, while a much broader line (labeled B) appears at the higher-energy side of the line A. This broad line B was also observed in $Y_2O_3:Eu^{3+}$ nanocrystals.[30]

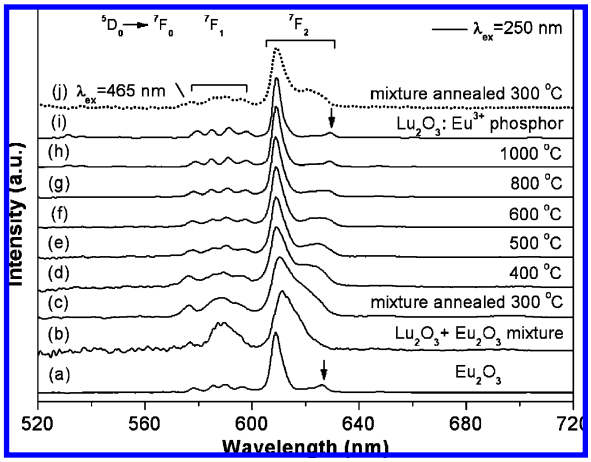

Figure 6. Emission spectra upon 250 nm excitation of cubic Eu_2O_3 powder (a), 98% cubic Lu_2O_3 + 2% cubic Eu_2O_3 mixed powder without annealing (b), and the mixture after annealing in air for 1 h at 300 °C (c), 400 °C (d), 500 °C (e), 600 °C (f), 800 °C (g), and 1000 °C (h) as well as Lu_2O_3:Eu^{3+} bulk powder (i). The emission spectrum of the 300 °C annealed mixture under 465 nm excitation is also presented (j).

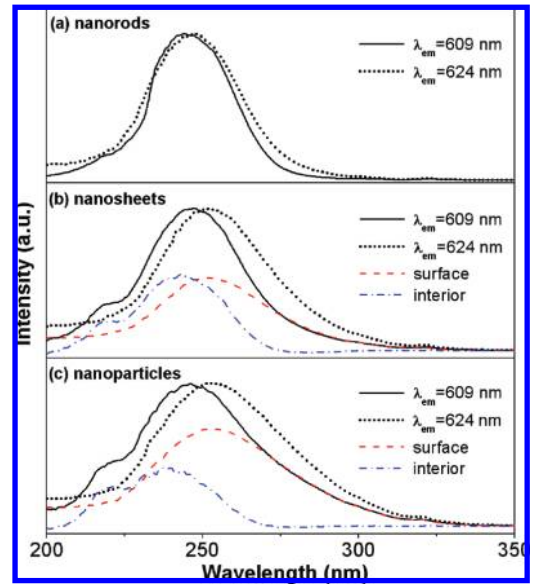

Figure 7. Excitation spectra by monitoring the 609 and 624 nm emission lines of Lu_2O_3:Eu^{3+} nanorods (a), nanosheets (b), and nanoparticles (c).

Regarding line A as an intrinsic environment of Lu_2O_3 host, line B reflects a novel environment generated in nanosized Lu_2O_3 host. The appearance of line B consequently leads to the blue shift and the enhancement of $^5D_0-{}^7F_0$ emission in the nanosamples, as shown in Figure 4. The broadening of both line A and B indicates the disordered environments in the nanocrystals. Furthermore, the environment for line B is more disordered. As we know, the $^5D_0-{}^7F_0$ transition can result from admixture of $4f^6 5d$ configuration to the $4f^7$ ground configuration via the linear odd crystal field.[31,32] Therefore, the more disordered environment may result in enhanced $^5D_0-{}^7F_0$ emission. Figure 5b shows the $^5D_0-{}^7F_2$ emission spectra under selective excitation within the $^7F_0-{}^5D_0$ absorption in the nanoparticles sample. One can find that the 624 nm emission line grows up as the excitation wavelength changes toward line B, demonstrating the similar spectral shape with that in Figure 4c. It is concluded that the line B, the 624 nm emission line, and the CTB long tail in the nanosamples relate to the same novel environment. Considering the enhanced effect of the novel environment with decreasing sample size, we speculate that the novel environment is related to the surface of the samples.

To confirm the assumption, we do the hereinafter experiments, and the results are shown in Figure 6. In the experiment, cubic Lu_2O_3 and Eu_2O_3 powder with average particle size of 50 nm are used. The cubic Eu_2O_3 powder shows a series of sharp lines of $^5D_0-{}^7F_{0,1,2}$ transitions (Figure 6a). After 2% mol of cubic Eu_2O_3 powder mixes with 98% mol of cubic Lu_2O_3 powder homogenously at room temperature, the emission spectrum of the mixture exhibits broad $^5D_0-{}^7F_{0,1,2}$ lines (Figure 6b) followed by a blue shift of the $^5D_0-{}^7F_0$ line and a red shift of the $^5D_0-{}^7F_2$ line. We have to attribute the spectral change to the surface effect of Eu_2O_3 particles, which are surrounded loosely by Lu_2O_3 particles. As the mixture is annealed at 300 °C for 1 h in air, the emission spectrum (Figure 6c) exhibits a strong shoulder at 624 nm and a further blue-shifted $^5D_0-{}^7F_0$ line. The spectral distribution is almost identical with that in Lu_2O_3:Eu^{3+} nanoparticles under 260−310 nm excitation, as shown in Figure 4c. As the annealing temperature is further raised, the shoulder at 624 nm becomes weak and the $^5D_0-{}^7F_2$ emission line at 609 nm becomes strong, while the $^5D_0-{}^7F_0$ line shifts back to the red. Finally, the spectrum trend is that in cubic Lu_2O_3:Eu^{3+} phosphor. This phenomenon actually reflects the thermal diffusion processes of Eu^{3+} from the surface to the inside of Lu_2O_3 particles. Annealed at 300 °C, Eu_2O_3 and Lu_2O_3 particles contact tightly rather than in the case of the mixture without annealing. Hence, the spectrum of the mixture annealed at 300 °C is responsible for the Eu^{3+} on the surface of Lu_2O_3 or in the interface between Lu_2O_3 and Eu_2O_3 phases. As the annealing temperature goes higher than 300 °C, more and more Eu^{3+} ions diffuse into the inside of Lu_2O_3 particles, resulting in reduced surface effect and instead enhanced interior behavior. It should be noted that the spectrum of Lu_2O_3:Eu^{3+} phosphor is different from that of Eu_2O_3 powder because the arrowed $^5D_0-{}^7F_2$ line is located at 630 nm in Lu_2O_3:Eu^{3+} and at 626 nm in Eu_2O_3. This indicates that the luminescence in Figure 6h originates from the interior Eu^{3+} of Lu_2O_3 rather than Eu_2O_3. The question left is where the interior luminescence of Eu_2O_3 particles is. In fact, Eu_2O_3 can strongly absorb UV excitation light due to CT transition. If the penetration depth of UV into Eu_2O_3 is less than the radius of an Eu_2O_3 particle, the luminescence of Eu_2O_3 under UV excitation is mainly contributed by the surface of Eu_2O_3 particles. It is therefore understood that the surface modification by mixing with Lu_2O_3 particles in the present work can remarkably change the luminescence of Eu_2O_3 particles.

In order to probe the interior luminescence of Eu_2O_3 particles in the mixture, the partially permitted $^7F_0-{}^5D_2$ transition of Eu^{3+} is excited at 465 nm for increasing penetration depth of the excitation light. It is found that the luminescence spectrum of pure Eu_2O_3 powder upon 465 nm excitation is exactly the same as that (Figure 6a) upon 250 nm UV excitation, indicating that the surface and the interior luminescence of pure Eu_2O_3 powder without surface modification are identical. Differently, the mixture exhibits both the surface (Figure 6c) and the interior (Figure 6a) characteristics upon 465 nm excitation. As an example, the emission spectrum upon 465 nm excitation of the mixture annealed at 300 °C is presented in Figure 6j.

Regarding the 609 and 624 nm lines as the interior Eu^{3+} and the surface Eu^{3+}, respectively, of Lu_2O_3:Eu^{3+} nanosamples, the excitation spectra are measured by monitoring the 609 and 624 nm emission lines, respectively, as shown in Figure 7. The CTB for the 624 nm line locates at the longer wavelength side of that for the 609 nm line in the nanosamples. Considering the

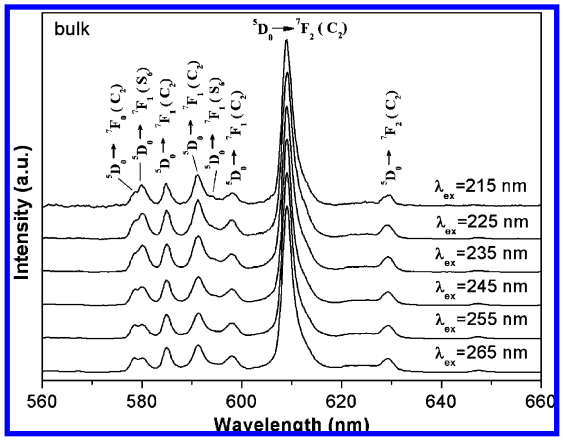

Figure 8. Emission spectra of Lu_2O_3:Eu^{3+} bulk sample excited by different wavelengths within its CTB.

sharpness of the 609 nm line and the broadness of the 624 nm line, we treat the excitation spectrum monitoring at the 624 nm line as the contribution of the surface Eu^{3+} only, and that monitoring at the 609 nm emission line as the superposition of the surface Eu^{3+} and the interior Eu^{3+}. Thereby, the excitation spectrum of the interior Eu^{3+} by spectral decomposition is obtained in the nanosheets and nanoparticles, as shown in parts b and c, respectively, of Figure 7. It is worth noting that the CTB of the interior Eu^{3+} presents an obvious blue shift compared to that of the bulk sample, while that of the surface Eu^{3+} shows a prominent red shift. In comparison with nanosheets, the CTBs of the surface Eu^{3+} and the interior Eu^{3+} in nanoparticles shift much more due to the smaller size, leading to a more visible broadening of the CTB. As a consequence, we infer for Eu^{3+}-doped nanocrystals that if the interior Eu^{3+} ions dominate the luminescence, the CTB for monitoring at 609 nm presents a blue shift due to the size confinement effects, as reported by Zhang et al.[15] In contrast, if the surface Eu^{3+} ions dominate the luminescence, the CTB for monitoring at 609 nm presents a red shift due to the distorted surface environments. If the competition between the two types of Eu^{3+} is coordinative, the CTB for monitoring at 609 nm may not show obvious shifts, only broadening, as in the present case. In view of this point, good crystallinity and large crystal size are favorable for luminescence of the interior Eu^{3+}. Disordered environments, low crystallinity, and small crystal size are favorable for luminescence of the surface Eu^{3+}.

In Figure 3a, it is obviously observed that the CTB of the bulk sample consists of two components separated from each other, which are located at about 230 and 245 nm, respectively. As we know, for cations, there exist two types of crystallographic sites in cubic Lu_2O_3 host, centrosymmetric S_6 site and noncentrosymmetric C_2 site, and the CTB is a superposition of the two components. In the isostructural Y_2O_3 host, it is reported that the CTBs of Eu^{3+} at the S_6 site are positioned slightly higher than that of Eu^{3+} at the C_2 site.[27,28] To further verify it, we measured the emission spectra upon CTB excitation with different wavelengths, as shown in Figure 8. It is clearly observed that the intensity ratio of $^5D_0-{}^7F_1$ (S_6) to $^5D_0-{}^7F_0$ (C_2) emission lines decreases as the excitation wavelength increases. This result suggests that in Lu_2O_3 host, as in Y_2O_3 host, the CTB of Eu^{3+} at the S_6 site locates at the high-energy side of Eu^{3+} at the C_2 site, so we attribute the shorter-wavelength constituent of the CTB to Eu^{3+} at the S_6 site and the other at the C_2 site. However, it is hard to observe the CTB of Eu^{3+} at the S_6 site in the nanocrystals due to the disorder structures. The number of the S_6 site and the symmetries of the sites are

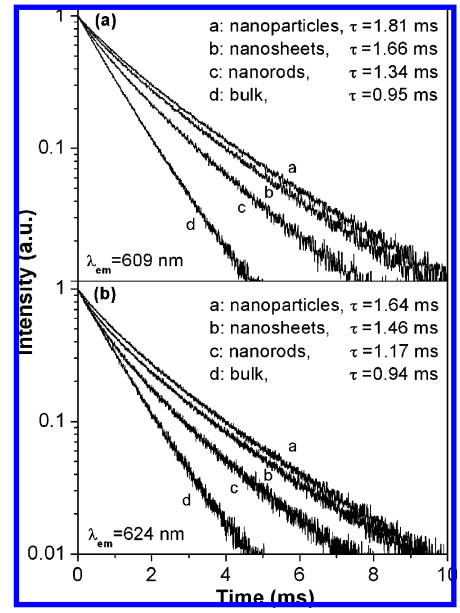

Figure 9. Fluorescence decay curves of the $^5D_0$ state of Lu_2O_3:Eu^{3+} nanocrystals and bulk sample: (a) the interior Eu^{3+} (λ_{em} = 609 nm); (b) the surface Eu^{3+} (λ_{em} = 624 nm).

both decreased strongly because of the disorder structures. However, we cannot observe the intensity reduction of the CTB around 230 nm in the nanocrystals. This is attributed to the blue shift of the CTB of the interior Eu^{3+} to compensate the spectrum. Another band located at about 217 nm is observed distinctly in nanocrystals. This band is attributed to the host absorption of Lu_2O_3 host exciton.[21,26] It is clearly noted that the host absorption bands in the excitation spectrum of the surface Eu^{3+} in the nanocrystals are annihilated strongly due to the imperfect surface lattice, so as a pure CTB is left. In the excitation spectra of the interior Eu^{3+}, the intensity ratios of the host absorption band to the CTB are enhanced notably with reduced sample size (see Figures 3a and 7). This is perhaps due to the more efficient energy transfer from the CT states than the exciton state of host to the luminescent killers in the nanosized samples. In the bulk sample, considering the negligible luminescent killers, the intense CTB may lead to an undetectable host exciton band.

C. Lifetimes. Parts a and b, respectively, of Figure 9 show the fluorescence decay curves for the interior Eu^{3+} (λ_{em} = 609 nm) and the surface Eu^{3+} (λ_{em} = 624 nm) in Lu_2O_3:Eu^{3+} nanocrystals excited by 266 nm nanosecond-pulsed laser. For comparison, we also measure the fluorescence decay curves of the bulk sample. In Figure 9, all decay curves exhibit nearly single-exponential behavior. The fluorescence lifetimes of the surface Eu^{3+} are shorter than that of the interior Eu^{3+} in nanocrystals. This is attributed to the luminescent killers on the surface. As expected, the two lifetimes in the bulk sample are almost the same due to the negligible surface effect. On examining the values of the lifetimes of the nanocrystals and bulk sample, one notices a lengthening of the lifetimes in the nanocrystals, and they are enhanced gradually with reduced sample size, which is consistent with the result reported by Boyer et al.[12] This behavior has been explained by Meltzer et al.[33] on the basis of changes in the refractive index of the surrounding medium of the Eu^{3+} ion as one goes to the nanometer size range.

IV. Conclusions

In conclusion, we synthesize cubic Lu_2O_3:Eu^{3+} nanorods, nanosheets, and nanoparticles via the hydrothermal approach

by adjusting the pH values of the precursor solutions. The luminescence properties of nanocrystals evidently show differences as compared to that of the micrometer-sized sintered counterparts. With decreasing samples sizes from the bulk sample to nanorods, nanosheets, and finally to nanoparticles, the CTBs of the samples are continuously broadened and followed by a longer and longer tail at the long-wavelength side; the relative intensity of the 624 nm emission line grows up gradually. The intrinsic line A in the excitation spectra by monitoring the $^5D_0-^7F_2$ emission and scanning the $^7F_0-^5D_0$ transition becomes broadened; moreover, a much broader line B appears at the higher-energy side of the intrinsic line A and becomes much stronger and further extends toward short wavelengths. Based on the experimental results of the thermal diffusion processes of Eu^{3+} from the surface to the inside of Lu_2O_3 particles, we conclude that the CTB long tail, the 624 nm emission line, and the broad line B all relate to the same novel environment, which originates from the surface Eu^{3+} of the nanocrystals. As the surface Eu^{3+} are selectively excited, the intensity ratio of the 624 nm emission line is enhanced notably, and the $^5D_0-^7F_0$ emission line also grows up and shifts to the high-energy side. By the spectral decomposition, we obtain the excitation spectra of the interior Eu^{3+} and the surface Eu^{3+} of nanocrystals. In comparison with the bulk sample, the CTB of the interior Eu^{3+} presents an obvious blue shift due to the size confinement effects, while that of the surface Eu^{3+} shows a prominent red shift due to the distorted surface environments. The lifetimes of the surface Eu^{3+} are all shorter than that of the interior Eu^{3+}, further indicating the distorted local environments on the surface of the nanocrystals. The results obtained here well explain the shifts and the broadening of the CTB in Eu^{3+}-doped nanocrystals.

Acknowledgment. This work is financially supported by the National Nature Science Foundation of China (10834006, 10774141) and the MOST of China (2006CB601104, 2006AA03A138).

References and Notes

(1) Lim, S. F.; Riehn, R.; Ryu, W. S.; Khanarian, N.; Tung, C.; Tank, D.; Austin, R. H. *Nano Lett.* **2006**, *6*, 169.
(2) Bai, X.; Song, H. W.; Pan, G. H.; Liu, Z. X.; Lu, S. Z.; Di, W. H.; Ren, X. G.; Lei, Y. Q.; Dai, Q. L.; Fan, L. B. *Appl. Phys. Lett.* **2006**, *88*, 143104.
(3) Si, R.; Zhang, Y. W.; Zhou, H. P.; Sun, L. D.; Yan, C. H. *Chem. Mater.* **2007**, *19*, 18.
(4) Zhang, Y. X.; Guo, J.; White, T.; Tan, T.; Xu, R. *J. Phys. Chem. C* **2007**, *111*, 7893.
(5) Matsuura, D. *Appl. Phys. Lett.* **2002**, *81*, 4526.
(6) Tao, Y.; Zhao, G. W.; Zhang, W. P.; Xia, S. D. *Mater. Res. Bull.* **1997**, *32*, 501.
(7) Tissue, B. M. *Chem. Mater.* **1998**, *10*, 2837.
(8) Williams, D. K.; Bihari, B.; Tissue, B. M.; McHale, J. M. *J. Phys. Chem. B* **1998**, *102*, 916.
(9) Igarashi, T.; Ihara, M.; Kusunoki, T.; Ohno, K.; Isobe, T.; Senna, M. *Appl. Phys. Lett.* **2000**, *76*, 1549.
(10) Qi, Z. M.; Shi, C. S.; Zhang, W. W.; Zhang, W. P.; Hu, T. D. *Appl. Phys. Lett.* **2002**, *81*, 2857.
(11) Jiang, X. C.; Yan, C. H.; Sun, L. D.; Wei, Z. G.; Liao, C. S. *J. Solid State Chem.* **2003**, *175*, 245.
(12) Boyer, J. C.; Vetrone, F.; Capobianco, J. A.; Speghini, A.; Bettinelli, M. *J. Phys. Chem. B* **2004**, *108*, 20137.
(13) Wang, J. C.; Liu, Q.; Liu, Q. F. *J. Mater. Chem.* **2005**, *15*, 4141.
(14) Qi, Z. M.; Liu, M.; Chen, Y. H.; Zhang, G. B.; Xu, M.; Shi, C. S.; Zhang, W. P.; Yin, M.; Xie, Y. N. *J. Phys. Chem. C* **2007**, *111*, 1945.
(15) Fu, Z. L.; Zhou, S. H.; Pan, T. Q.; Zhang, S. Y. *J. Lumin.* **2007**, *124*, 213.
(16) Boyer, J. C.; Gagnon, J.; Cuccia, L. A.; Capobianco, J. A. *Chem. Mater.* **2007**, *19*, 3358.
(17) Mao, Y. B.; Huang, J. Y.; Ostroumov, R.; Wang, K. L.; Chang, J. P. *J. Phys. Chem. C* **2008**, *112*, 2278.
(18) Li, Y. P.; Zhang, J. H.; Zhang, X.; Luo, Y. S.; Ren, X. G.; Zhao, H. F.; Wang, X. J.; Sun, L. D.; Yan, C. H. *J. Phys. Chem. C* **2009**, *113*, 4413.
(19) Vetrone, F.; Boyer, J. C.; Capobianco, J. A.; Speghini, A.; Bettinelli, M. *J. Phys. Chem. B* **2002**, *106*, 5622.
(20) Yang, J.; Li, C. X.; Quan, Z. W.; Zhang, C. M.; Yang, P. P.; Li, Y. Y.; Yu, C. C.; Lin, J. *J. Phys. Chem. C* **2008**, *112*, 12777.
(21) Zych, E.; Hreniak, D.; Strek, W. *J. Phys. Chem. B* **2002**, *106*, 3805.
(22) Lempicki, A.; Brecher, C.; Szupryczynski, P.; Lingertat, H.; Nagarkar, V. V.; Tipnis, S. V.; Miller, S. R. *Nucl. Instrum. Methods Phys. Res., Sect. A* **2002**, *488*, 579.
(23) Zych, E.; Trojan-Piegza, J. *Chem. Mater.* **2006**, *18*, 2194.
(24) Daldosso, M.; Sokolnicki, J.; Kepinski, L.; Legendziewicz, J.; Speghini, A.; Bettinelli, M. *J. Lumin.* **2007**, *122−123*, 858.
(25) Zych, E.; Wawrzyniak, M.; Kossek, A.; Trojan-Piegza, J.; Kępiński, L. *J. Alloys Compd.* **2008**, *451*, 591.
(26) Xu, M.; Zhang, W. P.; Dong, N.; Jiang, Y.; Tao, Y.; Yin, M. *J. Solid State Chem.* **2005**, *178*, 477.
(27) Jia, M. L.; Zhang, J, H.; Lu, S. Z.; Sun, J. T.; Luo, Y. S.; Ren, X. G.; Song, H. W.; Wang, X, J. *Chem. Phys. Lett.* **2004**, *384*, 193.
(28) Wang, C. N.; Zhang, W. P.; Yin, M. *J. Alloys Compd.* **2009**, *474*, 180.
(29) Li, Y. P.; Zhang, J. H.; Zhang, X.; Luo, Y. S.; Lu, S. Z.; Ren, X. G.; Wang, X. J.; Sun, L. D.; Yan, C. H. *Chem. Mater.* **2009**, *21*, 468.
(30) Peng, H. S.; Song, H. W.; Chen, B. J.; Lu, S. Z.; Huang, S. H. *Chem. Phys. Lett.* **2003**, *370*, 485.
(31) Kiss, Z. J.; Weakliem, H. A. *Phys. Rev. Lett.* **1965**, *15*, 457.
(32) Nieuwpoort, W. C.; Blasse, G. *Solid State Commun.* **1966**, *4*, 227.
(33) Meltzer, R. S.; Feofilov, S. P.; Tissue, B. M.; Yuan, H. B. *Phys. Rev. B* **1999**, *60*, R14012.

JP906738M